Millimeter Wave Spectrum Sharing using Analog True Time Delay Array based Wideband Nulling

Aditya Wadaskar*, Shamik Sarkar†, and Danijela Cabric*

*Department of Electrical and Computer Engineering, University of California Los Angeles, USA

†Department of Electronics and Communication Engineering, Indraprastha Institute of Information Technology Delhi, India
Email: adityaw@ucla.edu, shamik@iiitd.ac.in, danijela@ee.ucla.edu

Abstract-Millimeter wave (mmWave) cellular networks are characterized by dense deployments of base stations and users. Identifying spectrum-sharing opportunities in these bands is of crucial importance to ensure optimal spectrum utilization. However, non-cooperating cellular operators sharing spectral resources suffer from capacity degradation due to wideband interference. Without explicit channel knowledge and coordination across operators, interference suppression with the analog phased antenna arrays deployed by the mmWave antenna front end is difficult. In this context, this paper proposes a low-complexity and low-latency wideband nulling solution using analog True-Time-Delay arrays to facilitate spectrum sharing between operators. The proposed method does not require explicit channel estimation and strict coordination between operators and exploits the spatial degrees of freedom to achieve the desired beamforming and null steering, based on the estimated Angles of Arrival (AoA) of the incoming signals. We also present simulation results to demonstrate the interference suppression capabilities of the proposed algorithm, and provide comparison with digital arraybased algorithms.

Index terms—spectrum sharing, wideband nulling, millimeter wave, true time delay array

I. INTRODUCTION

Spectrum sharing has been identified as one of the key tools for dealing with the spectrum crunch problem in the sub-6 GHz bands. As cellular technology is evolving from the currently standardized 5G towards 6G, the bands above 6 GHz, particularly mmWave, are becoming extremely important. Hence, it is crucial to identify the opportunities for spectrum sharing in the mmWave bands. Recent work from Qualcomm on mmWave spectrum sharing between cellular operators reinforces this idea [1]. It advocates for multiple cellular operators to share spectrum resources to promote efficient dynamic utilization of the spectrum. With the help of coordinated spectrum sensing measurements, each operator opportunistically operates in spectra primarily used by other operators as long as the interference caused by the secondary operators of the spectrum to its natural incumbents falls below FCC-mandated thresholds.

In this work, we consider the problem of mmWave spectrum sharing without explicit coordination between two (or more) cellular operators in a given area [2]. This coexistence within the same spectrum without explicit coordination gives rise to

This work was supported by SpectrumX, which is an NSF Spectrum Innovation Center funded via Award 2132700.

interference that degrades sum rate [3]. In this context, we address the problem of interference management for millimeter wave cellular operators where the interference is caused by other coexisting shared-spectrum cellular operators.

The spatial sparsity of mmWave channels results in clustered interference channels. This allows exploitation of spatial degrees of freedom to implement beam nulling based on the Angles of Arrival (AoA) of the desired and interference signals. Such an approach requires the primary user to estimate only the AoA of the dominant desired and interference signal paths, thereby circumventing explicit wideband channel estimation. For the purpose of AoA estimation, each operator resorts to a coordinated uplink/downlink pilot exchange.

The analog phased arrays widely deployed in mmWave antenna array frontends are primarily used for directional beamforming to maximize gain along the desired AoA [4]. However, designing an analog combiner to achieve the required null steering without hurting the desired signal is challenging. Recent works in [5]–[7] have addressed this problem. The work in [5] presents a heuristic phased array design to create one null and a genetic optimization-based Nulli-Fi algorithm to successively null multiple interferers in a hardware-constraint-aware manner. The work in [6] proposes a reinforcement-learning (RL) based solution for agile null steering but incurs high training overhead. Additionally, since analog phased antenna arrays produce a frequency-flat spatial response, the works [5]–[7] are prone to beam-squint.

Analog True-Time-Delay (TTD) arrays, which can implement frequency-dependent beams using a single Radio Frequency (RF) chain [8], are an attractive candidate for beam-squint correction. When interference AoAs are known, Kronecker decomposition [7] of the TTD combiner is an effective way to steer multiple squint-free nulls without any optimization or learning. Additionally, TTD arrays can implement fully dispersive rainbow beam codebooks [9], [10] that can facilitate the expedited estimation of desired and interference AoA.

Therefore, to protect the primary operator from interference due to co-existing secondary users, we propose a low-complexity low-latency nulling beamforming solution that utilizes analog TTD arrays for fast AoA estimation and agile squint-free null steering via Kronecker Decomposition. The main contributions of the paper are summarized as follows:

• We derive in closed-form the design of TTD array param-

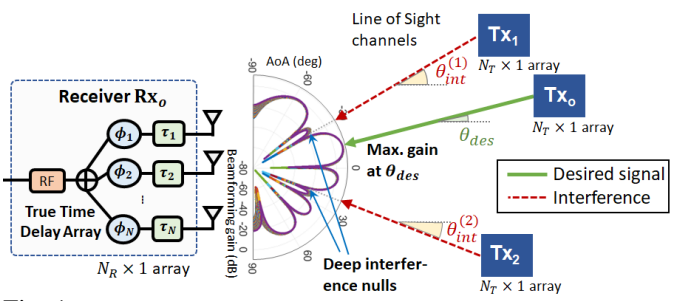


Fig. 1: System Model: A single user in a mmWave MIMO interference network with one desired signal source and I interferers.

eters (delays and phases) via Kronecker decomposition, to steer squint-free nulls at given interference AoA while maximizing gain at desired AoA (Sec III).

- We design the algorithm for low-latency high-accuracy multi-source interference AoA estimation using dispersive analog TTD codebook (Sec IV).
- We demonstrate via simulation results the interference suppression capabilities of the our solution to support spectrum sharing of cellular operators.

Notation: Scalars, vectors, and matrices are denoted by non-bold, bold lower-case, and bold upper-case letters, respectively. For a given matrix \mathbf{A} , $e^{\mathbf{A}}$ and $\log(\mathbf{A})$ denote matrices with the $(i,j)^{th}$ element given by $e^{A_{i,j}}$ and $\log A_{i,j}$ respectively. Conjugate, transpose and Hermitian transpose are denoted by $(.)^*$, $(.)^{\mathrm{T}}$, and $(.)^{\mathrm{H}}$ respectively.

II. SYSTEM MODEL AND PROBLEM FORMULATION

A. System Model

In this work, without loss of generality, we treat inter and intra-operator interference equally. We consider the interference management problem from the perspective of a single receiver Rx_0 in an mmWave cellular network, sharing its spectrum with I interfering transmitter-receiver pairs. Receiver Rx_0 , equipped with an $N_R \times 1$ antenna array, receives desired signals in the downlink from Tx_0 , and interference signals from $Tx_i \ \forall i=1,...,I$, where all $Tx_{i=0,...,I}$ are equipped with an $N_T \times 1$ antenna array, as shown in Fig. 1. All Tx-Rx pairs sharing the spectrum operate over bandwidth BW, and transmit/receive an Orthogonal Frequency Division Multiplexing (OFDM) signal with a total of M_{tot} subcarriers at carrier frequency f_c , where the frequency of the m^{th} subcarrier is given as follows.

$$f_{m} = f_{c} - \frac{BW}{2} - \frac{BW}{2M_{tot}} + \frac{m-1}{M_{tot}}BW \quad \forall \ m \in \{1, ..., M_{tot}\}$$
(1)

Each Tx_i node uses precoder $\mathbf{v}_i \in \mathbb{C}^{N_T \times 1}$ to transmit data and pilot signals to its respective Rx_i . The precoders \mathbf{v}_i are fixed and assumed to be known to the respective Tx_i . The frequency-dependent channel between Rx_0 and Tx_i is denoted by $\mathbf{H}_i[m] \in \mathbb{C}^{N_R \times N_T} \ \forall \ i=0,...,I$. Since mmWave channels are spatially sparse, we assume that the desired and interference signals arrive at Rx_0 in one dominant cluster (Line of Sight (LoS)). The geometric ray tracing representation of $\operatorname{H}_i[m]|_{i=0,...,1}$ can thus be expressed as follows:

$$\mathbf{H}_{i}[m] = \sum_{r=1}^{N_{\text{rays}}} \alpha_{i}^{r}[m] \mathbf{a}_{\text{rx}}(\theta_{i}^{R}(r), f_{m}) \mathbf{a}_{\text{tx}}^{H}(\theta_{i}^{T}(r), f_{m})$$
(2)

where $\alpha_i^r[m]$, $\theta_i^R(r)$ and $\theta_i^T(r)$ are the gain, AoA and Angle of Departure (AoD) of the r^{th} ray for $\mathbf{H}_i[m]$, where $r=1,...,N_{\text{rays}}$. $\mathbf{a}_{\text{tx}}(\theta,f_m)$ and $\mathbf{a}_{\text{rx}}(\theta,f_m)$ are the array response vectors at the Tx and Rx respectively, defined as follows.

$$\mathbf{a}_{tx}(\theta, f_m) = e^{j[0,\dots,N_T - 1]^T \pi \frac{f_m}{f_c} \sin \theta}$$

$$\mathbf{a}_{tx}(\theta, f_m) = e^{j[0,\dots,N_R - 1]^T \pi \frac{f_m}{f_c} \sin \theta}$$
(3)

Assuming LoS propagation with very small AoA spreads, the desired and interference AoA can be denoted as $\theta_{\text{des}} = \theta_0^R(r)$ and $\theta_{\text{int}}^{(j)}|_{j=1,...,I} = \theta_i^R(r) \ \forall r=1,...,N_{\text{rays}}.$

The Rx₀ deploys an analog TTD array with uniform half-wavelength spacing. Each antenna element is controlled with time delays and phase shifts, which are denoted by vectors $\mathbf{t}, \mathbf{p} \in \mathbb{R}^{N_R \times 1}$ respectively. The frequency-dependent combiner at the Rx $\mathbf{w}_{\text{TTD}}[m] \in \mathbb{C}^{N_R \times 1}$ is obtained as follows:

$$\mathbf{w}_{\text{TTD}}[m] = \frac{1}{\sqrt{N_T}} e^{-j(2\pi f_m \mathbf{t} - \mathbf{p})}$$
(4)

The received signal at Rx_o post combining is given as follows:

$$y[m] \in \mathbb{C} = \underbrace{\mathbf{w}_{\mathrm{TTD}}^{H}[m]\mathbf{H}_{0}[m]\mathbf{v}_{0}[m]x_{0}[m]}_{\mathrm{Desired: }y_{\mathrm{des}}[m]} + \underbrace{\mathbf{w}_{\mathrm{TTD}}^{H}[m]\mathbf{N}[m]}_{\mathrm{Noise}} + \underbrace{\sum_{i=1}^{I}\mathbf{w}_{\mathrm{TTD}}^{H}[m]\mathbf{H}_{i}[m]\mathbf{v}_{i}[m]x_{i}[m]}_{\mathrm{Interference: }y_{int}[m]}$$

where $\mathbb{E}[x_i[m]x_i^H[m]] = 1 \ \forall m, i, \ \mathbf{N}[m] \sim \mathcal{CN}(0, \sigma^2 \mathbf{I}_{N_R})$. The Signal to Interference and Noise Ratio (SINR) $\gamma[m]$ (post-combining) can computed from the desired signal and interference signal as follows.

$$\gamma[m] = \frac{\mathbb{E}[y_{des}y_{des}^H]}{\mathbb{E}[y_{int}y_{int}^H] + \mathbb{E}[\mathbf{w}_{TTD}^H[m]\mathbf{N}[m]]^2}$$
(6)

where $\gamma[m]$ is the SINR at the m^{th} subcarrier. At high SNR, the SINR becomes equivalent to the Signal to Interference Ratio (SIR) which indicates interference rejection capability.

B. Problem Statement and proposed approach

The goal is to design the delays \mathbf{t} and phase shifts \mathbf{p} to generate TTD combiner $\mathbf{w}_{\text{TTD}}[m]$ to maximize the spectral efficiency of Rx_0 , mathematically expressed as follows:

$$\{\mathbf{t}^{\star}, \mathbf{p}^{\star}\} = \underset{\mathbf{t}, \mathbf{p}}{\operatorname{arg\,max}} \quad \frac{1}{M_{tot}} \sum_{m=1}^{M_{tot}} \log_2 \left(1 + \gamma[m]\right) \quad (7)$$

The spectral efficiency maximization in (7) is equivalent to maximizing the desired signal power and minimizing interference (max-SINR). Traditionally, digital antenna arrays rely on complete channel knowledge to optimize the combiner coefficients. However, with analog TTD arrays, we do not have adequate degrees of freedom to optimize spectral efficiency per subcarrier. Since the desired and interference signals arrive in a single dominant cluster, we adopt a spatial alignment

approach to solve the max-SINR problem. Specifically, we attempt to design the delay and phase vectors of the TTD combiner so as to steer wideband nulls at interference AoAs, while maximizing beamforming gain along the desired AoA. Such an approach relies on the accurate estimation of desired and interference AoA.

III. AGILE WIDEBAND INTERFERENCE NULL STEERING VIA KRONECKER DECOMPOSITION

This section presents the Kronecker decomposition-based analog TTD combiner design to steer squint-free wideband nulls at the given $\{\theta_{int}^{(i)}|_{i=1,\dots,I}\}$, while maximizing the beamforming gain along the desired AoA θ_{des} , assuming that the AoA are perfectly known. The low-latency high-accuracy estimation of $\{\theta_{int}^{(i)}|_{i=1,\dots,I}\}$ and θ_{des} is explained in Sec. IV.

A. Kronecker Decomposition for wideband null steering

Under the special condition $N_R=2^K$ where $K\in\mathbb{Z}^+$, the TTD combiner $\mathbf{w}_{\mathrm{TTD}}[m]\in\mathbb{C}^{N_R\times 1}$ can be decomposed into $K=\log_2 N_R$ Kronecker factors [11] as follows.

$$\mathbf{w}_{\text{TTD}}[m] = \frac{1}{\sqrt{N_R}} \begin{bmatrix} 1 \\ e^{-j2\pi f_m \tau_1} e^{j\phi_1} \end{bmatrix} \otimes \dots \otimes \begin{bmatrix} 1 \\ e^{-j2\pi f_m \tau_K} e^{j\phi_K} \end{bmatrix}$$
(8)

where \otimes denotes the Kronecker product, and τ_i and ϕ_i are the delay and phase shift for the i^{th} Kronecker factor. Similarly, the Rx array response vector $\mathbf{a}_{\mathrm{rx}}(\theta, f_m) \in \mathbb{C}^{N_R \times 1}$ defined in (3) can be decomposed into K Kronecker factors as follows.

$$\mathbf{a}_{\text{rx}}(\theta, f_m) = \prod_{i=1}^{K} \begin{bmatrix} 1 \\ e^{j2^{K-i}\pi \frac{f_m}{f_c} \sin \theta} \end{bmatrix}$$
(9)

where \prod_{\otimes} denotes the Kronecker product of vectors. The beamforming gain at angle θ can thus be expressed as follows using properties of Kronecker product of vectors [11].

$$G(\theta, f_m) = |\mathbf{w}_{\text{TTD}}^H[m] \mathbf{a}_{\text{rx}}(\theta, f_m)|^2$$

$$= \left| \left(\prod_{i=1}^K \mathbf{w}_{\text{TTD}}^{(i)}[m] \right)^H \left(\prod_{i=1}^K \mathbf{a}_{\text{rx}}^{(i)}(\theta, f_m) \right) \right|^2$$

$$= \prod_{i=1}^K \left| \left(\mathbf{w}_{\text{TTD}}^{(i)}[m] \right)^H \mathbf{a}_{\text{rx}}^{(i)}(\theta, f_m) \right|^2$$
(10)

Thus, the K Kronecker factors of the TTD combiner can be visualized as the cascade of K frequency-spatial filters. The gain of the i^{th} spatial filter $F^{(i)}(\theta, f_m)$ is given as follows.

$$F^{(i)}(\theta, f_m) = \frac{1}{2} \left| 1 + e^{j\pi(2f_m\tau_i - \frac{\phi_i}{\pi} + \frac{f_m}{f_c} 2^{K-i} \sin \theta)} \right|^2$$
 (11)

Since the gains of the K spatial filters multiply to obtain the final beamforming gain, it is possible to use each of the K Kronecker factors to steer an independent wideband squint-free null or beam. For example, the i^{th} factor can be used to create a null at AoA $\theta_i \ \forall f_m$, by setting the delays τ_i as shown in (12) and phases $\phi_i = \pi$, as can be derived from (11). For the same τ_i , setting $\phi_i = 0$ steers a beam with gain maxima at θ_i .

$$\tau_i = -\frac{2^{K-i}\sin\theta_i}{2f_c} \; ; \; \phi_i = \begin{cases} \pi, & \text{steer null at } \theta_i \\ 0, & \text{beam maxima at } \theta_i \end{cases}$$
 (12)

It is important to note that the i^{th} Kronecker factor exhibits grating by a factor of 2^{K-i} , resulting in grating nulls. Setting τ_i as shown in (12) and $\phi_i = \pi$ would result in 2^{K-i} null copies at angles $\theta_{null}^{(i)}(q)$, $\forall q=1,...,2^{K-i}$, given as follows.

$$\theta_{null}^{(i)}(q) = \sin^{-1}\left(1 - \frac{q-1}{2^{K-i-1}} \frac{f_c}{f_m} - \text{mod}\left(1 - \sin\theta_i, 2\frac{f_c}{f_m}\right)\right)$$
(13)

This means that, a maximum of $\sum_{i=1}^{K} 2^{K-i} = 2^K - 1$ wideband nulls can be created using an $N_R \times 1$ array. Of these, only one null per Kronecker factor can be independently controlled.

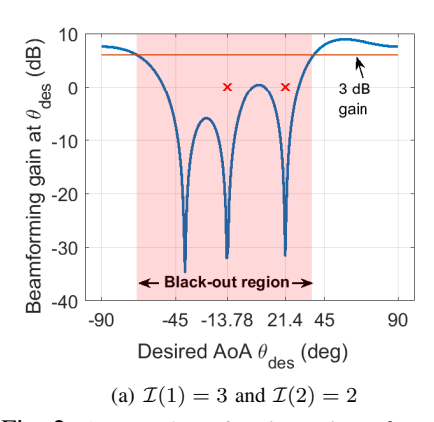
B. Optimal Kronecker factorization for given θ_{des} , $\theta_{int}^{(i)}|_{i=1,...,I}$

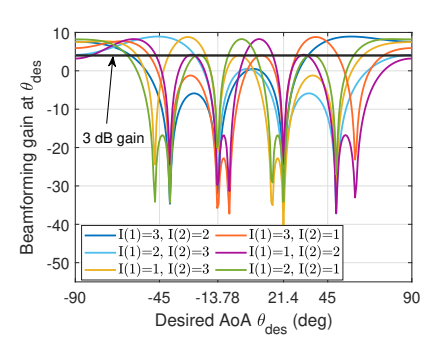
In addition to interference nulling, there needs to be a concerted effort to maximize the desired signal strength along $\theta_{\rm des}$. For I < K interference sources with AoA $\theta_{int}^{(i)}|_{i=1,\dots,I}$, it is sufficient to deploy any I Kronecker factors to steer wideband nulls in the required directions. The remaining K-I Kronecker factors must all be used to maximize beamforming gain along $\theta_{\rm des}$, achieved by setting τ_i as shown in (12) and $\phi_i = 0$. Since we need to reserve at least one factor for the desired signal, we can create at most $\log_2 N_R - 1$ independently controllable nulls using Kronecker decomposition.

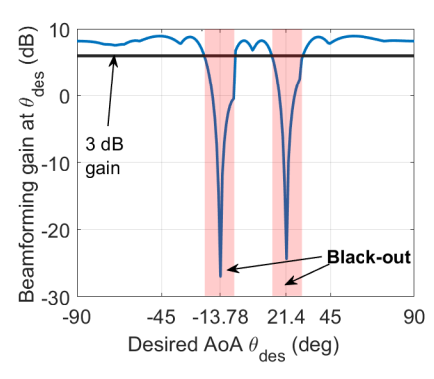
The indices of Kronecker factors chosen for nulling the I interferers affect the average beamforming gain in the desired direction $\frac{1}{M}\sum_{m}G(\theta_{des},f_{m})$. The mapping of $\theta_{int}^{(i)}$ to the factor index $k\in\{1,...,K\}$ is denoted by $\mathcal{I}(i)\in\{1,...,K\}$ $\forall i=1,...,I$. Given I< K interferers, there are $\frac{K!}{(K-I)!}$ possible mappings of I interferers to K factors. For given $\theta_{int}^{(i)}$, each $\theta_{int}^{(i)}\to\mathcal{I}(i)$ mapping or combination results in a range of AoA θ_{des} that never achieve good (e.g., >3dB) beamforming gain. We call this angular region the blackout region. This region depends on the interference AoA and their chosen nulling factors and is hence denoted as $\Theta_{X}(\theta_{int}^{(i)},\mathcal{I}(i)\big|_{i=1,...,I})$. Fig. 2(a) plots the average beamforming gain at θ_{des} as a

Fig. 2(a) plots the average beamforming gain at $\theta_{\rm des}$ as a function of θ_{des} , and illustrates the black-out region when the nulling combination $\mathcal{I}(1)=3$ and $\mathcal{I}(2)=2$ is used for $\{\theta_{int}^{(1)},\theta_{int}^{(2)}\}=\{-13.78^\circ,21.4^\circ\}$ for an 8×1 array. All angles in this region are unfavorable for desired signal reception. Fig. 2(b) plots the average beamforming gain $\frac{1}{M}\sum_m G(\theta_{des},f_m)$ for all 6 possible nulling combinations, where each combination is seen to have different favorable and unfavorable regions.

Depending on the value of θ_{des} and with the knowledge of $\{\theta_{int}^{(1)}, \theta_{int}^{(2)}\}$, it is possible to determine the *optimal nulling combination* which maximizes the beamforming gain at θ_{des} . Algorithm 1 presents a closed-form algorithm to determine the optimal Kronecker factor indices of the analog TTD combiner defined in (8) to null I given interferers while maximizing beamforming gain at θ_{des} . The derivation of (14) is provided in the Appendix. Fig. 2(c) plots $\frac{1}{M} \sum_m G(\theta_{des}, f_m)$ as a function of θ_{des} when the optimal nulling combination as

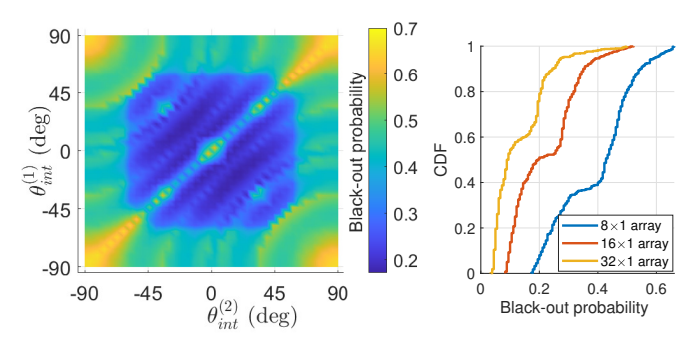






- (b) Beamforming gain vs. nulling choice
- (c) Optimal nulling combination

Fig. 2: Average beamforming gain at θ_{des} vs θ_{des} for 8×1 array, $\{\theta_{int}^{(1)}, \theta_{int}^{(2)}\} = \{-13.78^{\circ}, 21.4^{\circ}\}$. (a) Fixed nulling combination $\mathcal{I}(1) = 3$ and $\mathcal{I}(2) = 2$. (b) All possible nulling combinations. (c) Optimal nulling combination(Table 1).



(a) Black-out Probability $(N_R=8)$ (b) Black-out Probability CDF Fig. 3: (a) Black-out probability as a function of relative interferer locations with the optimal nulling combination (Table 1), for $N_R=8$, $K=3,~I=2,~\theta_{des}=0^\circ$. (b) CDF of black-out probability over 2500 realizations of $\{\theta_{int}^{(1)},\theta_{int}^{(2)}\}\in[-90^\circ,90^\circ]$.

Algorithm 1 Algorithm for optimal Kronecker decomposition.

Given:
$$N_R$$
, θ_{des} , $\{\theta_{int}^{(i)}\}\ \forall\ i=1,...,I$
Use $\{\mathcal{I}(i)\}^{th}$ factor to null $\theta_{int}^{(i)}\ \forall\ i=1,...,I$:
If $\exists\ \mathcal{I}(i)\in\{1,...,K\};\ \mathcal{I}(i)\neq\mathcal{I}(j)\ \forall i\neq j$, such that
$$\left|\prod_{i=1}^{I}\sin\left(\frac{2^{K-\mathcal{I}(i)}}{2}\pi\left(\sin\theta_{\mathrm{des}}-\sin\theta_{\mathrm{int}}^{(i)}\right)\right)\right|\geq\frac{1}{\sqrt{2}} \quad (14)$$

If multiple $\{\mathcal{I}(i)\}$ satisfy (14) – Select the combination that maximizes beamforming gain along θ_{des}

per (14) is used for each $\theta_{\rm des}$ for the example described in Fig. 2(a). The optimal Kronecker factorization significantly reduces the black-out region. The probability of a random $\theta_{\rm des}$ experiencing black-out is proportional to the angular width of the black-out region. The black-out probability depends on the relative AoA separations of the two interferers, as seen in Fig. 3(a), and on the array size, as seen in Fig. 3(b). For a given channel configuration, a larger array has a lower black-out probability owing to the smaller null-width [12, Chapt 22.7].

IV. HIGH ACCURACY INTERFERENCE AOA ESTIMATION

This section prescribes a low-latency high-accuracy estimation of $\hat{\theta}_{des}$ and $\{\hat{\theta}_{int}^{(i)}|_{i=1,...,I}\}$ using a fully dispersive TTD codebook. The estimation of desired and interference AoA requires the operators to coordinate their downlink pilot transmissions. Essentially, each $\operatorname{Tx}_i \ \forall i=0,...,I$ synchronously transmits on each subcarrier a time domain training sequence of length L+1, given by $\tilde{\mathbf{b}}_i \in \mathbb{C}^{1 \times (L+1)} = [\mathbf{b}_i \ 1] \ \forall \ i=0,...,I,$ where $\mathbf{b}_i \in \mathbb{C}^{1 \times L}$ are orthonormal pilot sequences (known to

the respective
$$Rx_i$$
), such that $\mathbf{b}_i \mathbf{b}_j^H = \begin{cases} 1 & i = j \\ 0 & \text{otherwise} \end{cases}$.

The coherent received signal samples (before combining) at the antenna array of Rx_0 , received over L+1 time-stamps, are denoted by $\mathbf{Y}[m] \in \mathbb{C}^{N_R \times (L+1)}$ and given as follows.

$$\mathbf{Y}[m] = \mathbf{H}_0[m]\mathbf{v}_0[m]\tilde{\mathbf{b}}_0 + \sum_{i=1}^{I} \mathbf{H}_i[m]\mathbf{v}_i[m]\tilde{\mathbf{b}}_i + \mathbf{N}[m]$$
(15)

We use a dispersive TTD codebook combiner $\mathbf{w}_{\mathrm{disp}}[m]$ with $\Delta \tau = 1/BW$ and $\Delta \phi = 0$ to map M subcarriers to M unique angles [9], enabling a single-shot scan of the entire angular space. The Rx₀ uses itime-domain pilot \mathbf{b}_0 to segregate the received signal $(\mathbf{w}_{\mathrm{disp}}^H[m]\mathbf{Y}[m] \in \mathbb{C}^{1 \times (L+1)})$ into desired and interference signals $(y_{\mathrm{des}}[m], y_{\mathrm{int}}[m] \in \mathbb{C})$ as shown below.

$$y_{\text{des}}[m] = \mathbf{w}_{\text{disp}}^{H}[\text{ m}]\mathbf{Y}[m] \underbrace{\begin{bmatrix} \mathbf{I}_{L} \\ \mathbf{0}_{1 \times L} \end{bmatrix} \boldsymbol{b}_{0}^{H}}_{\tilde{\mathbf{A}}_{\text{des}}}$$

$$y_{\text{int}}[m] = \mathbf{w}_{\text{disp}}^{H}[\text{ m}]\mathbf{Y}[m] \underbrace{\left(\begin{bmatrix} \mathbf{0}_{L \times 1} \\ 1 \end{bmatrix} - \begin{bmatrix} \mathbf{I}_{L} \\ \mathbf{0}_{1 \times L} \end{bmatrix} \boldsymbol{b}_{0}^{H} \right)}_{\tilde{\mathbf{A}}_{\text{int}}}$$
(16)

where $\tilde{\mathbf{A}}_{\mathrm{des}}$, $\tilde{\mathbf{A}}_{\mathrm{int}} \in \mathbb{C}^{(L+1)\times 1}$ are constant vectors as a function of pilot sequence \mathbf{b}_0 . We exploit the unique subcarrier angle mapping to construct from $y_{\mathrm{des}}[m]$ and $y_{\mathrm{int}}[m]$ the spatial profiles of the desired and interference signals, denoted by $\mathbf{y}_{\mathrm{des}} \in \mathbb{C}^{M\times 1}$ and $\mathbf{y}_{\mathrm{int}} \in \mathbb{C}^{M\times 1}$, and defined as follows.

$$\mathbf{y}_{\text{des}} = [y_{\text{des}}[1], ..., y_{\text{des}}[M]]^T \; ; \; \mathbf{y}_{\text{int}} = [y_{\text{int}}[1], ..., y_{\text{int}}[M]]^T$$
(17

The angular resolution of the desired and interference spatial

 $^{^{1}}$ Just as beam width is inversely proportional to array size N_{R} , so is null width, since nulls can be viewed as anti-beams

profiles \mathbf{y}_{des} and \mathbf{y}_{int} is limited by the number of subcarriers M deployed for beam training. Therefore, we construct a high-resolution dictionary of generalized beamforming gains in Q >> M directions, denoted by $\mathbf{B} \in \mathbb{R}^{M \times Q}$, as proposed in [13]. Each q^{th} column of \mathbf{B} denotes the generalized beamforming gains on M subcarriers at angle $\theta_q|_{q=1,\dots,Q}$, where the generalized gain on m^{th} subcarrier at angle θ_q , is given as follows.

$$[\boldsymbol{B}]_{m,q} = \left| \mathbf{w}_{\text{disp}}^{H}[m] \mathbf{a}_{rx} \left(\theta_{q}, f_{m} \right) \right|^{2}$$
 (18)

The proposed high-resolution dictionary \mathbf{B} thus extends the angular resolution of the TTD codebook. The high-resolution power-spatial profiles of the desired and interference signals, denoted by $\tilde{\mathbf{y}}_{des}$, $\tilde{\mathbf{y}}_{int} \in \mathbb{C}^{Q \times 1}$ respectively, are obtained from matrix \mathbf{B} as shown below.

$$\tilde{\mathbf{y}}_{\text{des}} = \mathbf{B}^H \mathbf{y}_{\text{des}} \quad ; \quad \tilde{\mathbf{y}}_{\text{int}} = \mathbf{B}^H \mathbf{y}_{\text{int}}$$
 (19)

Based on [13], the desired AoA $\hat{\theta}_{des}$ can be estimated with high accuracy as follows.

$$\hat{\theta}_{des} = \theta_{q^{\star}} \text{ s.t. } q^{\star} = \underset{q}{\operatorname{arg max}} |\mathbf{B}^{H} \mathbf{y}_{des}|$$
 (20)

Unlike the desired signal, the interference signal is multisource, and interference power-spatial profile \mathbf{y}_{int} likely has multiple peaks. The resolvability and accuracy of these peaks depends on the relative AoA separations of interference signals, making simple peak detection prone to errors in AoA estimation. Further, in the absence of per-antenna I/Q samples (owing to an analog array), several sophisticated multi-source AoA estimation algorithms such as [14], [15] cannot be deployed here. In view of this, we propose a two-stage algorithm using analog TTD receiver processing based on coarse peak detection and iterative refinement, for high-accuracy multisource interference AoA estimation.

A. Coarse estimation based on peak detection

As a first step, we perform simple peak-detection on the interference power-spatial profile $\tilde{\mathbf{y}}_{\text{int}}$ to obtain coarse estimates $\{\theta_{int}^{(i)}\}$. Since the interference is multi-source, the coarse estimates would have high errors, especially when interference AoA are not well separated in space and $\tilde{\mathbf{y}}_{\text{int}}$ exhibits indistinct or composite peaks.

B. Iterative Astral refinement for Interference estimates

This section presents an iterative algorithm to refine the coarse estimates obtained in Sec. IV-A. A good measure of the accuracy of the estimated $\{\hat{\theta}_{int}^{(i)}\}$ is the residual interference power $\sum_{m} |\mathbf{y}_{int}[m]|^2$ upon constructing optimal Kronecker combiner (as per (14)) with the estimated $\hat{\theta}_{des}$ and $\{\hat{\theta}_{int}^{(i)}\}$. The residual interference would have minima at the true interference AoA $\{\theta_{int}^{(i)^*}\}$. Therefore, we formulate the interference AoA refinement problem with the post-nulling residual interference power cost function, as follows:

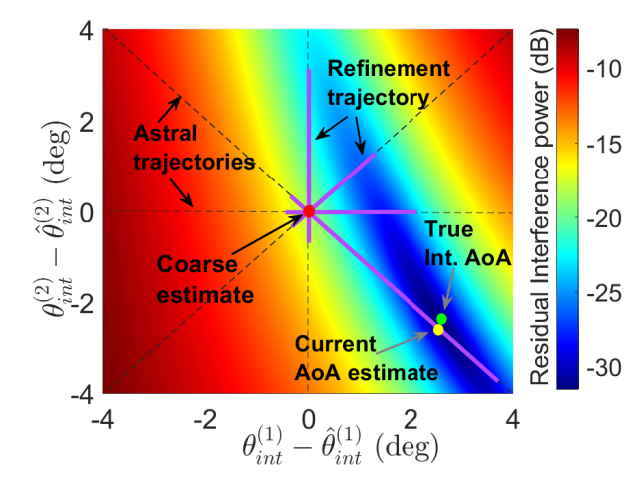


Fig. 4: Illustration of iterative Astral refinement of coarse estimates $\{\hat{\theta}_{int}^{(1,2)}\} = \{2.5^{\circ}, -17.64^{\circ}\}$ for $N_R = 8$, I = 2, $\theta_{des}^{\star} = -30^{\circ}$, and true interference AoA $\{0^{\circ}, -15^{\circ}\}$.

$$\{\theta_{int}^{(i)^{\star}}\} = \underset{\forall i \in \{1,..,I\}}{\operatorname{arg\,min}} \underbrace{\sum_{m} \left| \left(\mathbf{w}_{\text{opt}}(\theta_{des}, \theta_{int}^{(i)}, f_{m})\right)^{H} \mathbf{Y}[m] \tilde{\mathbf{A}}_{\text{int}} \right|^{2}}_{J(\theta_{des}, \{\theta_{\text{int}}^{(i)}\})}$$

$$(21)$$

where $\mathbf{w}_{\text{opt}}(\theta_{des}, \theta_{int}^{(i)}, f_m)$ is the optimal Kronecker combiner for the given desired and interference AoA.

Though the cost function is piecewise convex in the I-dimensional angular space in the neighborhood of the true AoA, performing Gradient Descent refinement of the coarse estimates is not possible. This is because the computation of the gradient step $\partial J/\partial\theta_{int}^{(i)}$, as shown in (22), relies on coherent samples $\mathbf{Y}[m]$ (in (15)), which the analog TTD array cannot provide.

$$\frac{\partial J}{\partial \theta_{int}^{(i)}} = \sum_{m} \mathbf{w}_{opt}^{H}[m] \mathbf{Y}[m] \tilde{\mathbf{A}}_{int} \tilde{\mathbf{A}}_{int}^{H} \mathbf{Y}^{H}[m] \frac{\partial \mathbf{w}_{opt}[m]}{\partial \theta_{int}^{(i)}}$$
(22)

With access to only received samples after combining $\mathbf{w}_{\text{opt}}^H[m]\mathbf{Y}[m]$, we propose an iterative refinement algorithm that perturbs coarse estimates $\{\hat{\theta}_{int}^{(i)}\}_{i=1,..,I}$ along fixed costminimizing trajectories emanating radially outward from the coarse estimate $\{\hat{\theta}_{int}^{(i)} \pm \xi^{(i)}\}|_{i=1,..,I}$ in an *I*-dimensional angular space, as shown in Fig. 4. Each refinement iteration performs the perturbation of estimates along the radial trajectories with a fixed step size. At each perturbation to point $\{\theta_{\text{iter}}^{(i)}\}$ $\forall i=1,...,I,$ the optimal nulling beam $\mathbf{w}_{\mathrm{opt}}(\hat{ heta}_{des}, heta_{\mathrm{iter}}^{(i)}, f_m)$ that steers nulls at $\{\theta_{\text{iter}}^{(i)}\}$ is used to measure the residual interference power and update the cost function. The perturbation along a particular trajectory is aborted if the cost function is found to increase along that trajectory. The point that minimizes the cost function across all perturbations in a particular iteration is treated as the radial center for the next refinement iteration, which proceeds with a refined perturbation step size to improve estimation accuracy. The iterative refinement of AoA estimates continues until the cost function-based stopping criterion is met.

Since the computation of the cost function requires succes-

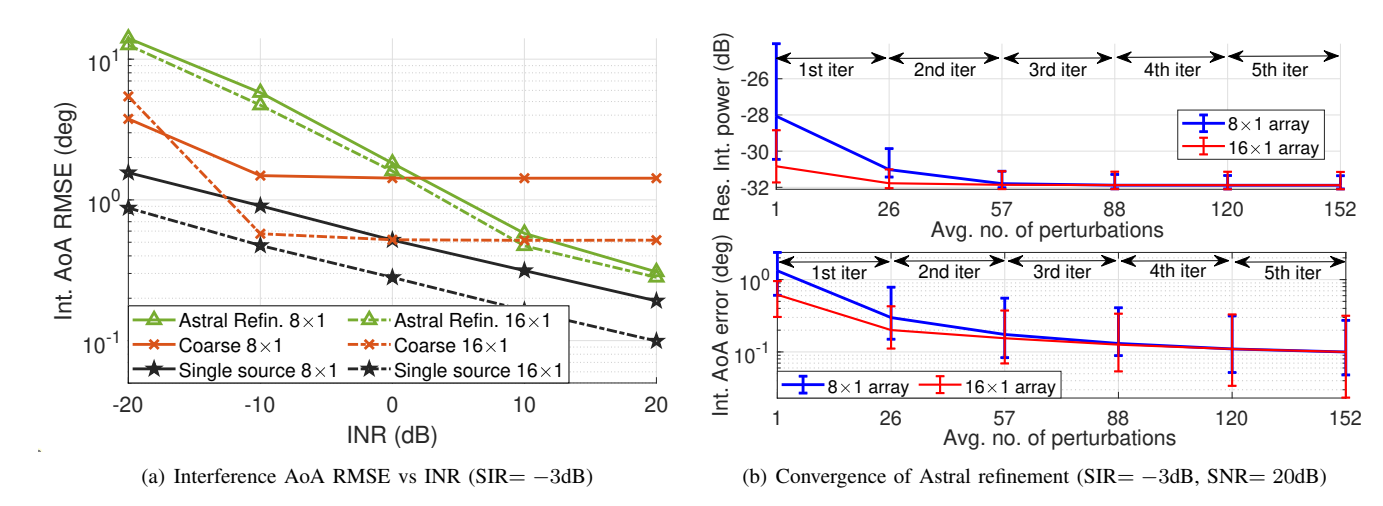


Fig. 5: (a) Interference AoA RMSE as a function of INR, and (b) Convergence of Astral refinement cost function and AoA estimation error for $N_R = 8$, 16, I = 2, $\theta_{des} = -30^{\circ}$, $\theta_{int}^{(1)} = 0^{\circ}$, averaged across 500 random interference AoA $\theta_{int}^{(2)} \in [-60^{\circ}, 60^{\circ}]$.

sive signal measurements with an updated beamformer at each perturbation, we assume that the interference does not change with time. Additionally, since the radial trajectories deployed resemble astral rays, we call this algorithm iterative Astral refinement. The variables of the algorithm are as follows.

- i. n: index of the n^{th} iteration
- ii. $\{\hat{\theta}_{int}^{(i,n)}\}|_{\forall i \in \{1,...,I\}}$: the current interference AoA estimates treated as the radial center in the n^{th} iteration.
- iii. $T = 3^{I} 1$ radially outward trajectories emanating from $\{\hat{\theta}_{int}^{(i,n)}\}|_{\forall i\in\{1,\dots,I\}}$ in an I-dimensional angular grid. iv. $\hat{p}^{(t)}\in\mathbb{R}^I$: directional vector of the t^{th} trajectory $\forall t=1,\dots,T$
- 1, ..., T, in the *I*-dimensional angular space with $\{\hat{\theta}_{int}^{(i,n)}\}$ as the origin. For example, for I = 2, the directional vectors $\hat{p}^{(t)} \ \forall \ t = 1, ..., 8$, are given by: [1,0], [1,1], [0,1], [-1,1], [-1,0], [-1,-1], [0,-1], [1,-1].
- v. $\Delta \theta^{(n)} = \frac{\epsilon}{2^{n-1}}$: perturbation step size in the n^{th} iteration, where ϵ is a constant. The angular increment at each perturbation along the t^{th} trajectory in the I-dimensional space is given by $\Delta \theta^{(n)} . \hat{p}^{(t)} \in \mathbb{R}^I = (\frac{\epsilon}{2^{n-1}}) . \hat{p}^{(t)}$.
- vi. ψ : Cost function based stopping criterion.

The detailed algorithm is summarized in Algorithm 2. Fig. 4 pictorially illustrates the refinement of coarse AoA estimates via perturbation along cost-minimizing astral trajectories. The heatmaps correspond to the residual interference power cost in (21), as a function of deviation from the coarse estimates, i.e. $\{\theta_{int}^{(i)} - \hat{\theta}_{int}^{(i)}\}$.

The final refined estimates $\{\hat{\theta}_{int}^{(i)}\}|_{i=1,...,I}$ are used to construct an optimal nulling TTD combiner $\mathbf{w}_{opt}[m]$ based on (14) and (12), thereby completing the proposed beam nulling solution. The complexity of the iterative Astral refinement algorithm is $\mathcal{O}(N_R(L+1)^2 M \cdot n_p)$, where n_p is the number of perturbations.

V. Numerical Results & Performance Analysis

This section presents numerical results to evaluate the interference suppression capability of the prescribed analog Algorithm 2 Astral refinement of coarse Interference AoA estimates

Given: N_R , I, $\hat{\theta}_{des}$, coarse Int. AoA estimates $\{\hat{\theta}_{int}^{(i)}\}|_{i=1,...,I}$ Initialization

- **1.** n=1 ; $\{\hat{\theta}_{int}^{(i,1)}\}=\{\hat{\theta}_{int}^{(i)}\}\ \forall i\in\{1,...,I\}$ **2.** 3^I-1 astral trajectories with directional vectors $\hat{p}^{(t)}\in\mathbb{R}^I$
- 3. Instantaneous cost gradient $\Delta J^{(1)} = J(\hat{\theta}_{des}, \{\hat{\theta}_{int}^{(i,1)}\})$

Iterate: While $\Delta J^{(n)} > \psi$

- **1.** $\Delta\theta^{(1)}=\frac{\epsilon}{2^{n-1}}$; Initial cost $J_{\text{init}}=J(\hat{\theta}_{des},\{\hat{\theta}_{int}^{(i,n)}\})$ **2.** For $t=1:1:3^I-1$ (perturb along 3^I-1 trajectories) abort = 0; $q_{iter} = 1$;

While abort==0

- Angle step: $\theta_{iter}^{(i)} = \theta_{int}^{(i,n)} + q_{iter} \Delta \theta^{(n)} \hat{p}^{(t)}(i)$
- Construct $\mathbf{w}_{\text{opt}}(\hat{\theta}_{des}, \theta_{iter}^{(i)}, f_m) \ \forall i \in \{1, ..., I\}$ $\implies \hat{y}_{\text{int}}[m] = \mathbf{w}_{\text{opt}}^{H}(\hat{\theta}_{des}, \theta_{iter}^{(i)}, f_{m})\mathbf{Y}[m]\tilde{\mathbf{A}}_{\text{int}}$
- Current cost: $J_{\text{curr}} = \sum_{m} |\hat{y}_{\text{int}}[m]|^2$
- Compute cost gradient $\Delta J_{\mathrm{iter}} = J_{\mathrm{curr}} J_{\mathrm{init}}$
- If $\Delta J_{\text{iter}} > 0$, abort = 1 (abort trajectory)
- If $\Delta^2 J_{\text{iter}} > 0$, record minima as potential AoA candidate; set abort = 1
- **vii.** $q_{\text{iter}} = q_{\text{iter}} + 1$; $J_{\text{init}} = J_{\text{curr}}$;

End While

End For

- 3. Update $\{\hat{\theta}_{int}^{(i,n+1)}\}|_{i=1,...,I}$ to the lowest minima recorded on refinement trajectory.
- **4.** $\Delta J^{(n+1)} = J(\hat{\theta}_{des}, \{\hat{\theta}_{int}^{(i,n)}\}) J(\hat{\theta}_{des}, \{\hat{\theta}_{int}^{(i,n+1)}\})$
- **5.** n = n + 1;

End While

TTD-based beam nulling solution. The receiver Rx₀ receives LoS desired signal from $\theta_{des}=-30^\circ$, and LoS interference from $\theta_{int}^{(2)}=0^\circ$ and $\{\theta_{int}^{(2)}\}\in[-60^\circ,60^\circ]\ (I=2)$. The other system parameters are as follows: $f_c=28\mathrm{GHz}$, $BW = 800 \text{MHz}, M_{tot} = 2048, \text{ pilot length } L = 32.$ The dispersive TTD codebook for beam training uses delays: $\mathbf{t} = [0,...,N_R-1]^T \frac{1}{BW}$, phases $\mathbf{p} = \mathbf{0}_{N_R \times 1}$, and $M = M_{tot}$ subcarriers. The high-resolution codebook has Q=8192

generalized directions. Astral refinement is performed for 5 iterations, with $\Delta\theta=0.25^\circ/2^{n-1}$ in the n^{th} iteration. The SNR (pre-combining) is 20dB and the SIR (pre-combining) is -3dB wherever unspecified. All results are averaged across 500 realizations where $\{\theta_{int}^{(2)}\}$ sweeps over $[-60^\circ,60^\circ]$. Table I summarizes the LoS desired and interference channel parameters used for simulations.

Parameter	Notation	Values
Tx array size	N_T	8, 16
Rx array size	N_R	8, 16
Desired AoA	$ heta_{ m des}$	-30°
No. of Interferers	I	2
Interference AoA	$ heta_{ ext{int}}^{(1)}$	0°
	$ heta_{ ext{int}}^{(2)}$	$\in [-60^{\circ}, 60^{\circ}]$

TABLE I: Desired and interference channel parameters for numerical results.

A. Estimation accuracy and convergence of Astral refinement

We evaluate the interference AoA estimation accuracy as a function of Interference-to-Noise Ratio (INR), which is expressed as INR (dB) = SNR (dB) - SIR (dB) (all precombining). Fig. 5(a) depicts the root-mean-squared-error (RMSE) of the coarse and refined estimates $\{\hat{\theta}_{int}^{(i)}\}$ (averaged for both angles) as a function of the INR, for the 8×1 (solid line) and 16×1 (dashed line) array. The black curves depict the AoA estimation RMSE for a single-source LoS signal (I = 1)received without any interference, and depict the lowest RMSE attainable with the proposed method. The coarse estimates for the 8×1 array have high RMSE (> 1°) even at high INR, for reasons already discussed in Sec. IV-A. Astral refinement is seen to considerably decrease AoA RMSE for INR > 10dB, but exhibits higher RMSE than coarse estimates at low INR. This is because high noise power relative to interference hampers the reliable computation of the residual interference power cost function across successive perturbations of the coarse estimates, leading to convergence issues of the proposed minima-seeking astral refinement. Further, a larger array (eg. 16×1) produces more accurate coarse estimates compared to a smaller array (eg. 8×1) owing to narrower codebook beams and increased antenna gain.

Fig. 5(b) depicts the convergence of astral refinement cost function and AoA estimation error (median across observations) at SNR=20dB and SIR=-3 dB, as a function of the total number of perturbations (or measurements), averaged across the 500 realizations with variable $\{\theta_{int}^{(2)}\} \in [-60^\circ, 60^\circ]$. At high INR, the 16×1 array results in faster convergence of cost as well as AoA error relative to the 8×1 array, due to more accurate coarse estimates which helps reduce several refinement steps.

B. Interference suppression capability

This section evaluates the interference suppression capability of the optimal TTD nulling beams $\mathbf{w}_{\text{opt}}[m]$ constructed

using the refined AoA estimates from Sec. IV-B as per (14), in terms of spectral efficiency.

As benchmarks for performance comparison, we consider the following beamforming solutions

1) Digital combiner with perfect CSI: With perfect knowledge of the channels $\mathbf{H}_i[m] \ \forall \ i=0,...,I$, the optimal digital combiner can be formulated as the minimization of the cost function $J(\mathbf{w},m)=1/\hat{\gamma}[m]$, as shown below.

$$\mathbf{w}_{\text{dig}}[m] = \underset{\mathbf{w} \in \mathbb{C}^{N_R \times 1}}{\operatorname{arg\,min}} \underbrace{\frac{\mathbf{w}^H \left(\hat{\mathbf{H}}_{\text{int}}[m] \hat{\mathbf{H}}_{\text{int}}^H[m] + \mathbf{R}\right) \mathbf{w}}{\mathbf{w}^H \mathbf{H}_0[m] \mathbf{v}_0[m] \mathbf{v}_0^H[m] \mathbf{H}_0^H[m] \mathbf{w}}}_{J(\mathbf{w}, m)}$$
(23)

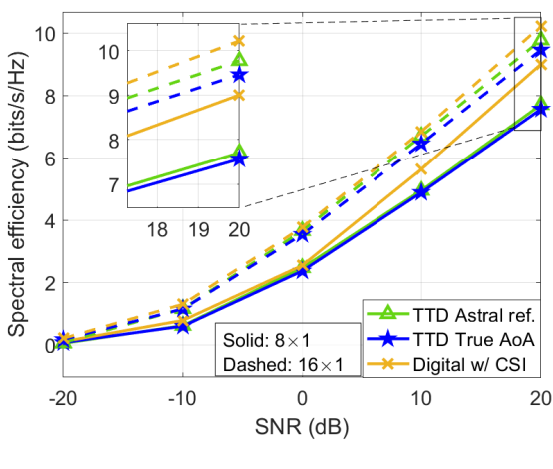
where, $\hat{\mathbf{H}}_{\mathrm{int}}[m] = \sum_{i \neq 0} \mathbf{H}_i[m] \mathbf{v}_i[m]$, and $\mathbf{R}[m] \in \mathbb{C}^{N_R \times N_R}$ is the noise covariance matrix. The digital combiner $\mathbf{w}_{\mathrm{dig}}$ can be obtained via gradient descent minimization as shown in the Appendix.

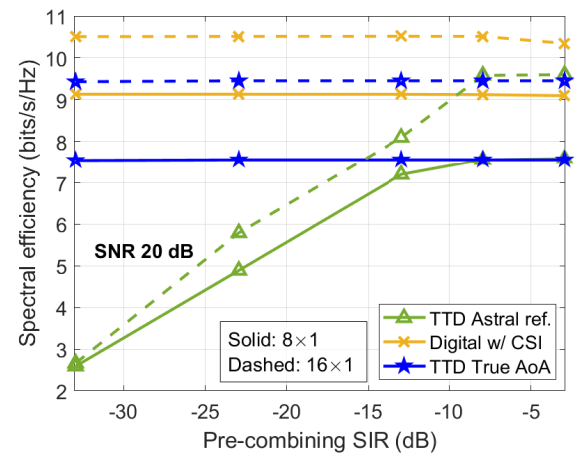
2) TTD True AoA: Corresponds to $\mathbf{w}_{opt}[m]$ constructed with true AoAs, assuming that the desired and interference AoA are perfectly known.

Fig. 6(a) plots the average spectral efficiency as a function of SNR for 8×1 array (solid line) and 16×1 array (dashed line), for SIR -3dB. We see that TTD Astral ref achieves comparable spectral efficiency to Digital w/ CSI for low and intermediate SNR \leq 0dB, but is outperformed by the latter at high SNR for both array sizes. It is worthwhile to note that the 16×1 array considerably reduces the performance gap between TTD Astral ref and Digital w/ CSI at high SNR relative to the 8×1 array. This can be attributed to the higher accuracy of AoA estimates, reduced probability of black-out, and increased array gain that the 16×1 array offers relative to 8×1 . Further, the comparable performance of TTD Astral ref and TTD True AoA at all SNR re-emphasizes the accuracy of AoA estimates with Astral refinement.

Fig. 6(b) plots average spectral efficiency across realizations as a function of pre-combining SIR, which denotes the extent of interference relative to the desired signal, for an SNR of 20dB. We see that TTD Astral ref. suffers significant degradation relative to Digital w/ CSI at very low SIR ≤ -15 dB, even though the interference AoA RMSE is small at low SIR (For SIR=-23dB, INR = SNR-SIR = 43dB, for which interference AoA errors are expected to be very small based on Fig. 5). Here, it is worthwhile to note that TTD True AoA does not suffer from a similar degradation, and achieves the same spectral efficiency at all studied SIR. This indicates that TTD Astral ref is highly sensitive to even very small errors in interference AoA estimates when the interference is very strong relative to the desired signal (very low SIR). TTD True AoA also depicts the spectral efficiency upper bound that can be achieved with Kronecker decomposition-based analog TTD combiners when the signal AoA are known perfectly. TTD Astral ref matches this upper bound of TTD True AoA when SIR> -10dB, thereby indicating that TTD Astral ref. performs well in moderately interference-rich channels.

Fig. 7 shows the CDF of the spectral efficiency for SNR





(a) Spectral efficiency vs SNR (SIR=-3dB)

(b) Spectral efficiency vs SIR (SNR= 20dB)

Fig. 6: Performance comparison of TTD Astral ref. with TTD True AoA and Digital w/ CSI for I=2, $\theta_{des}=-30^{\circ}$, $\theta_{int}^{(1)}=0^{\circ}$ averaged across $\theta_{int}^{(2)} \in [-60^{\circ}, 60^{\circ}]$.

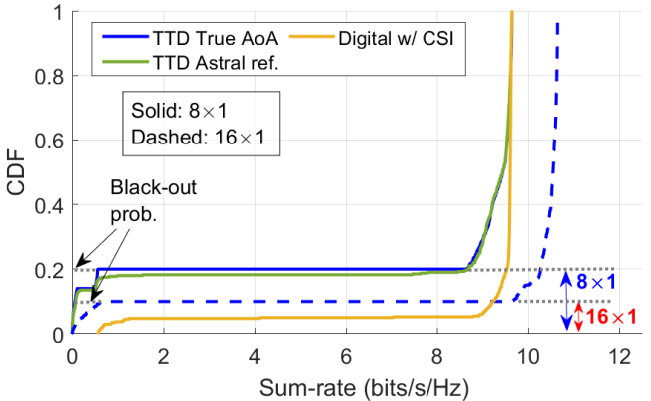


Fig. 7: Performance comparison of TTD beamforming with digital MSE for $I=2,~\theta_{des}=-30^\circ,~\theta_{int}^{(1)}=0^\circ$ averaged across $\theta_{int}^{(2)}\in[-60^\circ,60^\circ].~\mathrm{SNR}=20\mathrm{dB},~\mathrm{SIR}=-3\mathrm{dB}.$

20dB and pre-combining SIR -3dB for 8×1 array. Digital w/ CSI is seen to achieve the highest spectral efficiency at all instances. TTD-based nulling methods (Astral ref. and True AoA) have almost identical CDFs, indicating the efficacy of the AoA estimation deployed. Both TTD approaches are seen to suffer from black-out degradation with a probability of $\sim 20\%$, which reflects in highly degraded/recessed spectral efficiency. This black-out phenomenon, as discussed earlier, is an inherent limitation of Kronecker decomposition-based null steering, which occurs when either $\theta_{\rm des}$ falls in the close vicinity of one of $\theta_{\rm int}^{(1)}$ and $\theta_{\rm int}^{(2)}$, or when $\theta_{\rm int}^{(1)}$ and $\theta_{\text{int}}^{(2)}$ are too close. Interestingly, Digital w/ CSI also suffers from a small but prominent black-out probability ($\sim 5\%$). Barring the instances of black-out, TTD Astral ref. and TTD True AoA achieve comparable spectral efficiency compared to Digital w/o CSI with $\sim 45\%$ probability for 8×1 array. This establishes that the performance of TTD Astral ref/True AoA is highly dependent on the spatial/angular configuration of interference signals relative to each other. The deeply recessed tail of the CDF owing to black-out is instrumental in decreasing the average spectral efficiency of TTD-based methods in Fig. 6(a,b). However, increasing the array size to 16×1 (dashed blue curve) is seen to significantly reduce the black-out probability to $\sim 10\%$, and also improves spectral efficiency relative to 8×1 array.

Thus, in clustered interference channels, a spatial nulling approach via accurate interference AoA estimation and agile wideband nulling offers a promising low-cost low-complexity interference management technique that matches the performance of digital arrays in certain spatial channel configurations. Further, a larger array exhibits greater robustness to the stated limitations (black-out) and consequently improved performance in a larger set of channel configurations.

In real-world deployments, an operator, (here, receiver) whose desired signal arrival path coincides with or lies in the angular vicinity of the interference signal path, cannot be served with the required gain, owing to the null that must be inevitably steered for interference suppression. All interference-aware beamforming solutions would suffer from this black-out in some form. To facilitate interference-free communication with black-out afflicted users, the Rx needs to deploy advanced time/frequency domain scheduling and power control with the help of orthonormal pilot sequences. Such efforts, however, would add to the algorithm's complexity. We will explore how to circumvent black-out-related degradation in our future work. Additionally, since the approach works on a snapshot-by-snapshot basis, it can take care of mobility of interferers as well.

VI. CONCLUSIONS

This paper addresses the problem of interference management for cellular operators sharing spectrum resources in mmWave bands. In particular, we propose an interference management solution that requires limited coordination amongst operators, and exploits channel sparsity at super-6 GHz to implement spatial beam nulling. The proposed solution deploys analog TTD arrays to implement low-complexity wideband beam nulling using closed form expressions based on desired

and interference signal AoA. The paper also proposes a fast multi-source interference AoA estimation algorithm with astral refinement, which is shown to achieve highly accurate AoA estimates at intermediate and high INR. The proposed solution is shown to achieve a comparable sum-rate to methods deploying digital combiners with perfect channel knowledge. Though the proposed analog TTD combiner-based interference nulling suffers from black-out degradation, deploying larger arrays helps overcome this degradation considerably. The numerical results strongly advocate for deploying the proposed spatial alignment-based nulling as a promising interference management solution to enable inter- and intra-operator spectrum sharing in mmWave bands.

REFERENCES

- [1] "How a new millimeter wave spectrum sharing paradigm provides highly reliable connectivity and massive throughput gains," https://www.qualcomm.com/news/onq/2022/07/how-a-new-millimeter-wave-spectrum-sharing-paradigm-provides-hig.
- [2] H. Shokri-Ghadikolaei, F. Boccardi, C. Fischione, G. Fodor, and M. Zorzi, "Spectrum sharing in mmwave cellular networks via cell association, coordination, and beamforming," *IEEE Journal on Selected Areas in Communications*, vol. 34, no. 11, pp. 2902–2917, 2016.
- [3] V. Boljanovic, S. Sarkar, and D. Cabric, "Millimeter-wave user association and low-interference beam scheduling," in *Proceedings of the 6th ACM Workshop on Millimeter-Wave and Terahertz Networks and Sensing Systems*, 2022, pp. 7–12.
- [4] R. W. Heath, N. González-Prelcic, S. Rangan, W. Roh, and A. M. Sayeed, "An overview of signal processing techniques for millimeter wave mimo systems," *IEEE Journal of Selected Topics in Signal Processing*, vol. 10, no. 3, pp. 436–453, 2016.
- [5] S. Madani, S. Jog, J. O. Lacruz, J. Widmer, and H. Hassanieh, "Practical null steering in millimeter wave networks," in 18th USENIX Symposium on Networked Systems Design and Implementation (NSDI 21). USENIX Association, Apr. 2021, pp. 903–921. [Online]. Available: https://www.usenix.org/conference/nsdi21/presentation/madani
- [6] Y. Zhang, T. Osman, and A. Alkhateeb, "Online beam learning with interference nulling for millimeter wave mimo systems," *IEEE Trans*actions on Wireless Communications, pp. 1–1, 2023.
- [7] G. Zhu, K. Huang, V. K. N. Lau, B. Xia, X. Li, and S. Zhang, "Hybrid beamforming via the kronecker decomposition for the millimeter-wave massive mimo systems," *IEEE Journal on Selected Areas in Communications*, vol. 35, no. 9, pp. 2097–2114, 2017.
- [8] V. Boljanovic, H. Yan, E. Ghaderi, D. Heo, S. Gupta, and D. Cabric, "Design of millimeter-wave single-shot beam training for true-timedelay array," in 2020 IEEE 21st International Workshop on Signal Processing Advances in Wireless Communications, 2020, pp. 1–5.
- [9] H. Yan, V. Boljanovic, and D. Cabric, "Wideband millimeter-wave beam training with true-time-delay array architecture," in 2019 53rd Asilomar Conference on Signals, Systems, and Computers, 2019, pp. 1447–1452.
- [10] A. Wadaskar, V. Boljanovic, H. Yan, and D. Cabric, "3d rainbow beam design for fast beam training with true-time-delay arrays in wideband millimeter-wave systems," in 2021 55th Asilomar Conference on Signals, Systems, and Computers, 2021, pp. 85–92.
- [11] C. F. Loan, "The ubiquitous kronecker product," Journal of Computational and Applied Mathematics, vol. 123, no. 1, pp. 85–100, 2000, numerical Analysis 2000. Vol. III: Linear Algebra. [Online]. Available: https://www.sciencedirect.com/science/article/pii/ S0377042700003939
- [12] S. J. Orfinidas, Electromagnetic Waves and Antennas, (accessed in Dec 1, 2019). [Online]. Available: http://eceweb1.rutgers.edu/~orfanidi/ewa/ ewa-1up.pdf
- [13] V. Boljanovic, H. Yan, C.-C. Lin, S. Mohapatra, D. Heo, S. Gupta, and D. Cabric, "Fast beam training with true-time-delay arrays in wideband millimeter-wave systems," *IEEE Transactions on Circuits and Systems I: Regular Papers*, vol. 68, no. 4, pp. 1727–1739, 2021.
- [14] X. Zhou, F. Zhu, Y. Jiang, X. Zhou, W. Tan, and M. Huang, "The simulation analysis of doa estimation based on music algorithm," in 2020 5th International Conference on Mechanical, Control and Computer Engineering (ICMCCE), 2020, pp. 1483–1486.

[15] M. Wagner, Y. Park, and P. Gerstoft, "Gridless doa estimation and root-music for non-uniform linear arrays," *IEEE Transactions on Signal Processing*, vol. 69, pp. 2144–2157, 2021.

APPENDIX

A. Derivation of Optimal Kronecker factorization (14):

The goal is to determine the best mapping of $\theta_{int}^{(i)}$ to I nulling factor indices $\mathcal{I}(i) \ \forall \ i=1,...,I$, to maximize the beamforming gain at θ_{des} . The K-I desired signal factors are designed to achieve maximum gain at θ_{des} . The spatial filter gain at θ_{des} from the nulling factors for the given mapping $\mathcal{I}(i)$ is obtained as follows

$$G_{\text{null}}(\theta_{des}, f_m) = \frac{1}{2^I} \prod_{i=1}^{I} \left| 1 - e^{j2^{K-\mathcal{I}(i)} \pi \frac{f_m}{f_c} (\sin \theta_{des} - \sin \theta_{int}^{(i)})} \right|^2$$

$$= \frac{1}{2^I} \prod_{i=1}^{I} \left| -2j \sin \left(\frac{\alpha(i)}{2} \right) e^{j\frac{\alpha(i)}{2}} \right|^2 = \frac{1}{2^I} \prod_{i=1}^{I} \left| 2 \sin \left(\frac{\alpha(i)}{2} \right) \right|^2$$
(24)

where $\alpha(i) = 2^{K-\mathcal{I}(i)}\pi(\sin\theta_{des} - \sin\theta_{int}^{(i)})$. To achieve at least 3 dB gain at θ_{des} , the following equation must be satisfied.

$$G_{\text{null}}(\theta_{des}, f_m) = \frac{1}{2^I} \prod_{i=1}^I \left| 2 \sin\left(\frac{\alpha(i)}{2}\right) \right|^2 \ge 2^{I-1}$$

$$\implies \frac{1}{2^{I/2}} \prod_{i=1}^I \left| 2 \sin\left(\frac{\alpha(i)}{2}\right) \right| \ge \frac{2^{I/2}}{\sqrt{2}}$$

$$\implies \prod_{i=1}^I \left| \sin\left(\frac{\alpha(i)}{2}\right) \right| = \left| \prod_{i=1}^I \sin\left(\frac{\alpha(i)}{2}\right) \right| \ge \frac{1}{\sqrt{2}}$$

$$(25)$$

Substituting $\alpha(i)$ into (25) gives us (14).

B. Gradient Descent optimization of digital combiner (23):

The gradient step for the cost function $J(\mathbf{w}, m)$ can be obtained as follows:

$$\frac{\partial J(\mathbf{w}, m)}{\partial \mathbf{w}} = \frac{\mathbf{w}^{H}(\hat{\mathbf{H}}_{int}[m]\hat{\mathbf{H}}_{int}^{H}[m] + \mathbf{R})}{\mathbf{w}^{H}\mathbf{H}_{0}[m]\mathbf{v}_{0}[m]\mathbf{v}_{0}^{H}[m]\mathbf{H}_{0}^{H}[m]\mathbf{w}} \\
- \frac{\left(\mathbf{w}^{H}(\hat{\mathbf{H}}_{int}[m]\hat{\mathbf{H}}_{int}^{H}[m] + \mathbf{R})\mathbf{w}\right)\mathbf{w}^{H}\mathbf{H}_{0}[m]\mathbf{v}_{0}[m]\mathbf{v}_{0}^{H}[m]\mathbf{H}_{0}^{H}[m]}{|\mathbf{w}^{H}\mathbf{H}_{0}[m]\mathbf{v}_{0}[m]\mathbf{v}_{0}^{H}[m]\mathbf{H}_{0}^{H}[m]\mathbf{w}|^{2}} \tag{26}$$

Consequently, the optimal digital combiner is iteratively updated as follows, where n denotes the iteration index.

$$\mathbf{w}_{\text{dig}}^{(n+1)}[m] = \mathbf{w}_{\text{dig}}^{(n)}[m] - \mu \frac{\partial J(\mathbf{w}^{(n)}, m)}{\partial \mathbf{w}} \quad \forall n \ge 1$$
 (27)

where μ is a constant. The starting point $\mathbf{w}^{(0)} \in \mathbb{C}^{N_R \times 1}$ is chosen as a random unit-norm vector.